Journal of the Korean Crystal Growth and Crystal Technology
Vol. 19, No. 3 (2009) 107-115

Theoretical gravity studies on roles of convection in crystal growth of Hg_2Cl_2-Xe by physical vapor transport under normal and high gravity environments

Geug-Tae Kim† and Moo Hyun Kwon*

Department of Nano-Bio Chemical Engineering, Hannam University, Taejon 305-811, Korea
**Department of Applied Chemistry, Woosuk University, Wanju-gun 565-701, Korea*

(Received April 14, 2009)
(Accepted April 24, 2009)

Abstract Particular interest in the role of convection in vapor crystal growth has arisen since some single crystals under high gravity acceleration of $10g_0$ appear considerably larger than those under normal gravity acceleration ($1g_0$). For both $\Delta T = 60$ K and 90 K, the mass flux increases by a factor of 3 with increasing the gravity acceleration from $1g_0$ up to $10g_0$. On the other hand, for $\Delta T = 30$ K, the flux is increased by a factor of 1.36 for the range of $1g_0 \le g \le 10g_0$. The maximum growth rates for $1g_0$, $4g_0$, $10g_0$ appear approximately in the neighborhood of $y = 0.5$, and the growth rates shows asymmetrical patterns, which indicate the occurrence of either one single or more than one convective cell. The maximum growth rate for $10g_0$ is nearly greater than that for $1g_0$ by a factor of 2.0 at $P_B = 20$ Torr. For three different gravity levels of $1g_0$, $4g_0$ and $10g_0$, the maximum growth rates are greater than the minimum rates by a factor of nearly 3.0, based on $P_B = 20$ Torr. The mass flux increases with increasing the gravity acceleration, for $1g_0 \le g_y \le 10g_0$, and decreases with increasing the partial pressure of component B, xenon (Xe), P_B. The $|U|_{max}$ is directly proportional to the gravity acceleration for 20 Torr $\le P_B \le$ 300 Torr. As the partial pressure of P_B (Torr) decreases from 300 Torr to 20 Torr, the slopes of the $|U|_{max}$s versus the gravity accelerations increase from 0.1 sec to 0.17 sec. The mass flux of Hg_2Cl_2 is exponentially decayed with increasing the partial pressure of component B, P_B (Torr) from 20 Torr up to 300 Torr.

Key words Mercurous chloride, Convection, Xenon, gravity, Physical vapor transport

1. Introduction

Physical vapor transport (PVT) has become an important crystal growth process for a variety of acousto-optic materials. The mechanism of the PVT process is simple: sublimation-condensation in closed silica glass ampoules in temperature gradient imposed between the source material and the growing crystal. It also requires minimal process control and monitoring, and transport results are easily interpreted. Of particular importance is the use of PVT for materials processing experiments in low and high gravity environments, which would provide a better and thorough understanding of transport phenomena occurring in the vapor phase and crystal growth phenomena.

Over the past 25 years many theoretical modeling studies [1-12] on transport phenomena in PVT and much quantitative experiments [13-20] have been extensively investigated. Most important theoretical works were achieved by Rosenberger [1-4, 6, 8] and, recently extended for transition to chaos flow fields in specialty materials of mercurous chloride in applications of microgravity experiments by Duval [21-25]. They have addressed the underlying phenomena in the PVT processes on the relative importance and influencing parameters of diffusion-advection, thermal and/or solutal convection on mass transport. Our recent studies [26-33] are for PVT processes of specialty materials such as mercurous halides (Hg_2Cl_2 and Hg_2Br_2) under normal and microgravity environments to investigate the role of convection on the mass transport rate and its transition from diffusion-dominated to circulatory convection-dominated regimes in relation to total pressure, temperatures of source and crystal ends, aspect ratio (transport length-to-width), molecular weights, wall temperature profiles.

It is the purpose of this paper to study systematically the transport phenomena covering the various gravity accelerations in the PVT processes of Hg_2Cl_2 crystal growth system. For this theoretical analysis of the PVT processes, a two-dimensional model is in horizontally oriented, cylindrical, closed ampoules in a two-zone furnace system. Diffusion-limited processes are considered in this paper, although Singh, Mazelsky and Glicksman [34] demonstrated that the interface kinetics plays an important

†Corresponding author
Tel: +82-42-629-8837
Fax: +82-42-629-8835
E-mail: gtkim@hnu.kr

role in the PVT system of Hg_2Cl_2. The effects of normal and high gravity accelerations on solutally and/or thermally buoyancy-driven convection will be considered at this point, primarily for a mixture of Hg_2Cl_2 vapor and impurity of Xenon (Xe), although for gaining insights into the convection, the low gravity environments are more important than high gravity conditions in some cases.

2. The Model

Mercurous chloride (Hg_2Cl_2) materials are important for applications in acousto-optic and opto-electronic devices such as Bragg cells, X-ray detectors operating at ambient temperature [35]. The equimolar Hg_2Cl_2 compound decomposes to two liquids at a temperature near 525°C where the vapor pressure is above 20 atm [36, 37]. Because of this decomposition and high vapor pressure, Hg_2Cl_2 cannot be solidified as a single crystal directly from the stoichiometric melt. However, very similar to the mercurous bromide, mercurous chloride exhibits sufficiently high vapor pressure at low temperatures so that these crystals are usually grown by the physical vapor transport (PVT) in closed silica glass ampoules.

Consider a rectangular enclosure of height H and transport length L, shown in Fig. 1. The source is maintained at a temperature T_s, while the growing crystal is at a temperature T_c, with $T_s > T_c$. PVT of the transported component A (Hg_2Cl_2) occurs inevitably, due to presence of impurities, with the presence of a component B (Xe). The interfaces are assumed to be flat for simplicity. The finite normal velocities at the interfaces can be expressed by Stefan flow deduced from the one-dimensional diffusion-limited model [38], which would provide the coupling between the fluid dynamics and species calculations. On the other hand, the tangential component of the mass average velocity of the vapor at the interfaces vanishes. Thermodynamic equilibria are assumed at the interfaces so that the mass fractions at the interfaces are kept constant at $\omega_{A,s}$ and $\omega_{A,c}$. On the vertical non-reacting walls appropriate velocity boundary conditions are no-slip, the normal concentration gradients are zero, and wall temperatures are imposed as nonlinear temperature gradients. Thermo-physical properties of the fluid are assumed to be constant, except for the density. When the Boussinesq approximation is invoked, density is assumed constant except the buoyancy body force term. The density is assumed to be a function of both temperature and concentration. The ideal gas law and Dalton's law of partial pressures are used. Viscous energy dissipation and the Soret-Dufour (thermo-diffusion) effects can be neglected, as their contributions remain relatively insignificant for the conditions encountered in our PVT crystal growth processes. The transport of fluid within a rectangular PVT crystal growth reactor is governed by a system of elliptic, coupled conservation equations for mass (continuity), momentum, energy and species (diffusion) can be represented by the generic Eq. (1) [39] with their appropriate boundary conditions Eqs. (2) through (4). Let u_x, u_y denote the velocity components along the x- and y-coordinates in the x, y rectangular coordinate, and let T, ω_A, p denote the temperature, mass fraction of species A (Hg_2Cl_2) and pressure, respectively, where the superscript of * denotes the dimensionless [26-33].

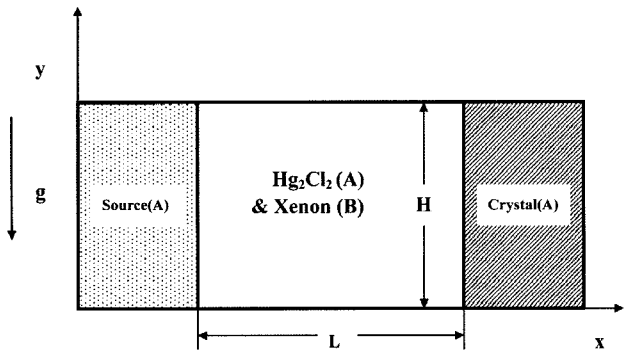

Fig. 1. Schematic and coordinates for a PVT crystal growth reactor of Hg_2Cl_2-Xe in a two-dimensional rectangular system.

$$\nabla\bullet(\rho u\phi) = \nabla\bullet(\Gamma\nabla\phi) + S, \tag{1}$$

On the walls ($0 < x^* < L/H$, $y^* = 0$ and 1):

$$u^*(x^*,0) = u^*(x^*,1) = v^*(x^*,0) = v^*(x^*,1) = 0 \tag{2}$$

$$\frac{\partial\omega_A^*(x^*,0)}{\partial y^*} = \frac{\partial\omega_A^*(x^*,1)}{\partial y^*} = 0,$$

$$T^*(x^*,0) = T^*(x^*,1) = \frac{T - T_c}{T_s - T_c}$$

On the source ($x^* = 0$, $0 < y^* < 1$):

$$u^*(0,y^*) = -\frac{1}{Le(1-\omega_{A,s})}\frac{\Delta\omega}{}\frac{\partial\omega_A^*(0,y^*)}{\partial x^*}, \tag{3}$$

$$v^*(0,y^*) = 0,$$
$$T^*(0,y^*) = 1,$$
$$\omega_A^*(0,y^*) = 1.$$

On the crystal ($x^* = L/H$, $0 < y^* < 1$):

$$u^*(L/H,y^*) = -\frac{1}{Le(1-\omega_{A,c})}\frac{\Delta\omega}{}\frac{\partial\omega_A^*(L/H,y^*)}{\partial x^*}, \tag{4}$$

$$v^*(L/H,y^*) = 0,$$
$$T^*(L/H,y^*) = 0,$$
$$\omega_A^*(L/H,y^*) = 0.$$

The vapor pressure [10] p_A of Hg_2Cl_2 (in the unit of Pascal) can be evaluated from the

$$p_A = e^{(a - b/T)}, \quad (5)$$

following formula as a function of temperature: in which a = 29.75, b = 11767.1.

3. Results and Discussion

The purposes for this study is to correlate the growth rate and the convective intensity to process parameters such as (1) temperature differences between the source and the crystal region, (2) partial pressures of component B (Xe), (3) normal and high gravitational levels to investigate the effects of noble inert gas Xe on the convection during physical vapor transport. Thus, it is desirable to express some results in terms of dimensional growth rate, however they are also applicable to parameter ranges over which the process varies in the manner given. The six dimensionless parameters, namely Gr, Ar, Pr, Le, C_v and Pe, are independent and arise naturally from the dimensionless governing equations and boundary conditions. The dimensionless parameters and physical properties for the operating conditions of this study are shown in Table 1.

Because the molecular weight of a noble element xenon (Xe) is not equal to that of the crystal component (Hg_2Cl_2) during the physical vapor transport, both

Table 1
Typical thermo-physical properties used in this study (M_A = 472.086, M_B = 131.3)

Transport length, L	10 cm
Height, H	2 cm
Source temperature, T_s	350°C
Crystal temperature, T_c	260°C
Density, ρ	0.002 g/cm^3
Dynamic viscosity, μ	0.00033 g/(cm · sec)
Diffusivity, D_{AB}	0.36 cm^2/s
Thermal expansion coefficient, β	0.0016 K^{-1}
Prandtl number, Pr	0.78
Lewis number, Le	0.5
Peclet, Pe	4.13
Concentration number, C_v	1.1
Total system pressure, P_T	413.06 Torr
Partial pressure of component B, P_B	20 Torr
Thermal Grashof number, Gr_t	5.6×10^4
Solutal Grashof number, Gr_s	4.0×10^5

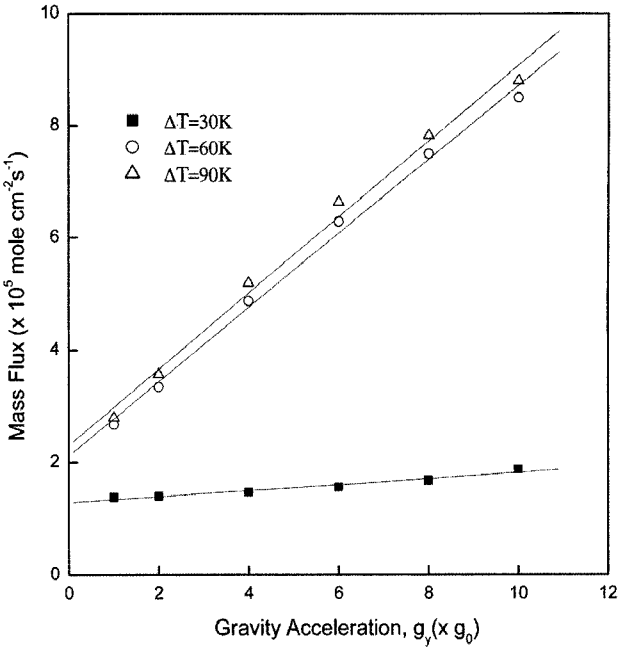

Fig. 2. The mass flux of Hg_2Cl_2 in terms of mole $cm^{-2}s^{-1}$ versus gravity acceleration in terms of g_0 (981 cm s^{-2}) for the horizontal orientations for three temperature differences between the source and the crystal regions: 320°C → 290°C (symbol ■), 350°C → 290°C (symbol ○), and 350°C → 260°C (symbol △). Based on Ar = 5, P_B = 20 Torr, Ar = 5, L = 10 cm, with the linear temperature profiles at walls.

solutal and/or thermal effects should be considered in this study. The linear temperature profiles at wall boundary conditions only are considered.

Fig. 2 shows the mass flux of Hg_2Cl_2 in terms of mole $cm^{-2}s^{-1}$ versus gravity acceleration in terms of g_0 (981 cm s^{-2}) for the horizontal orientations for three temperature differences between the source and the crystal regions: 320°C → 290°C (symbol ■), 350°C → 290°C (symbol ○), and 350°C → 260°C (symbol △). Based on the parameters of Ar = 5, P_B = 20 Torr, Ar = 5, L = 10 cm, with the linear temperatures on the walls. For ΔT = 90 K and $g_y = 1g_0$, the governing dimensionless parameters are as follows: aspect ratio Ar = 5.0, Prandtl number Pr = 0.78, Lewis number Le = 0.5, thermal Grashof number $Gr_t = 5.6 \times 10^4$, solutal Grashof number $Gr_s = 4.0 \times 10^5$, Peclet number Pe = 4.13, concentration number C_v = 1.1. Here, the subscript of 0 denotes the normal gravity acceleration of 981 cm • s^{-2}. For both ΔT = 60 K and 90 K, the mass flux increases by a factor of 3 with increasing the gravity acceleration from $1g_0$ up to $10g_0$. On the other hand, for ΔT = 30 K, the flux is increased by a factor of 1.36 for the range of $1g_0 \le g \le 10g_0$. As shown in Fig. 2, the variation in the flux when increasing the temperature difference from 60 K to up 90 K is insignificant, but important when

increasing from 30 K to 60 K. It is likely to be due to the presence of a sharp increase in total pressure with the corresponding source temperature. In other words, the source temperatures for both $\Delta T = 60$ K and 90 K are 350°C, and 320°C for $\Delta T = 30$ K, respectively. Consequently, under the conditions of gravity accelerations, the mass fluxes for both $\Delta T = 60$ K and 90 K are approximately greater than the flux at $\Delta T = 30$ K by a factor of 2. Although the graph for $T_s = 350$°C is not shown here, to prove our inference, comparisons of mass fluxes for $T_s = 320$°C and 350°C are made. To be specific, the mass flux at $T_s = 320$°C and $1g_0$ is 1.38×10^{-5} mole cm^{-2} s^{-1}; at $T_s = 350$°C and $1g_0$, 2.26×10^{-5} mole cm^{-2} s^{-1}. For $T_s = 350$°C, the mass flux at $1g_0$ is 1.87×10^{-5} mole cm^{-2} s^{-1}; at $10g_0$, 6.87×10^{-5} mole cm^{-2} s^{-1}. It is concluded the mass fluxes versus gravity accelerations vary with a relatively similar slope under the condition of same source temperature of 350°C. Note in actual crystal experiments the typical source and crystal temperature correspond to 320°C and 290°C, respectively.

Fig. 3 shows the $|U|_{max}$ as a function of gravity acceleration for the three temperature differences between the source and the crystal regions, corresponding to Fig. 2. The $|U|_{max}$ is the dimensional maximum magnitude of the velocity vector, which indicates the intensity of convection in the vapor phase. Fig. 3 illustrates the $|U|_{max}$ is a direct proportional and linear relationship with the gravity acceleration. The three cases of T = 30 K, 60 K, and 90 K have a gradient of 0.17, 0.27, and 0.29 cm s^{-1} g_0^{-1}, respectively. The $|U|_{max}$ is not increased by a factor of 2 as the temperature difference is increased by a factor of 2, but increased by a factor of 1.59 from $\Delta T = 30$ K to 60 K, and after $\Delta T = 60$ K increased by a factor of 1.07 until the temperature difference reaches $\Delta T = 90$ K.

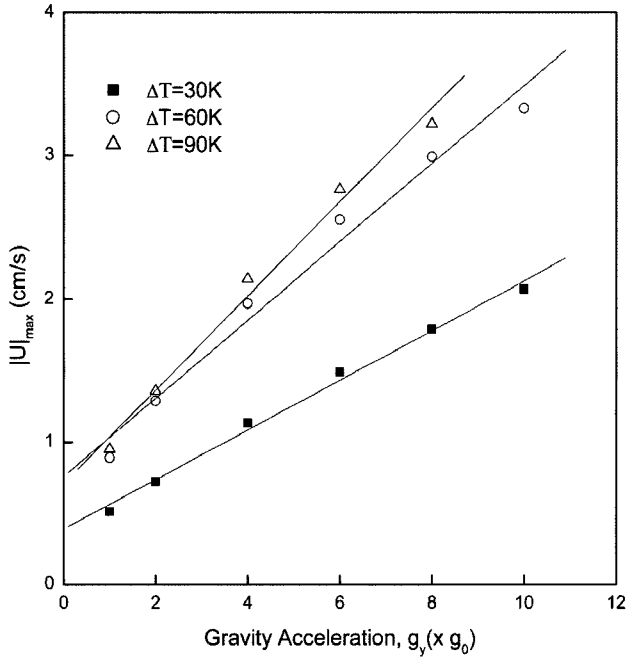

Fig. 3. The $|U|_{max}$ as a function of gravity acceleration for the three temperature differences between the source and the crystal regions, corresponding to Fig. 2.

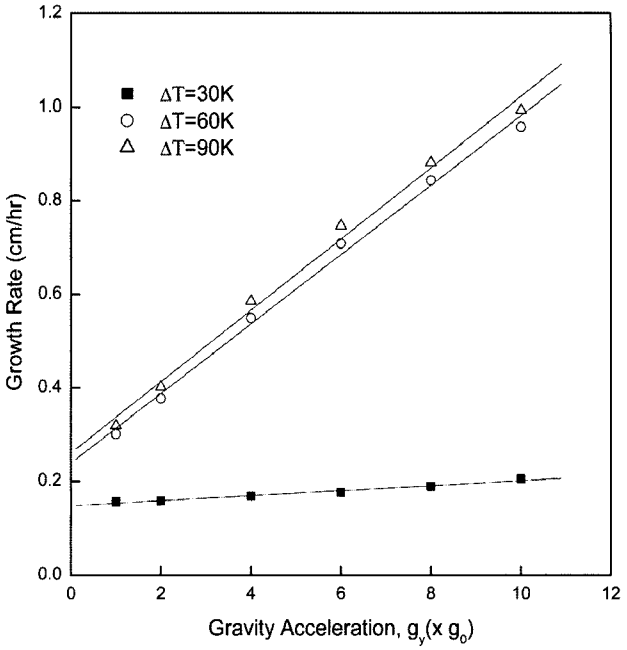

Fig. 4. Relationships between the growth rate and the gravity accelerations for three temperature differences between the source and the crystal regions, corresponding to Fig. 2.

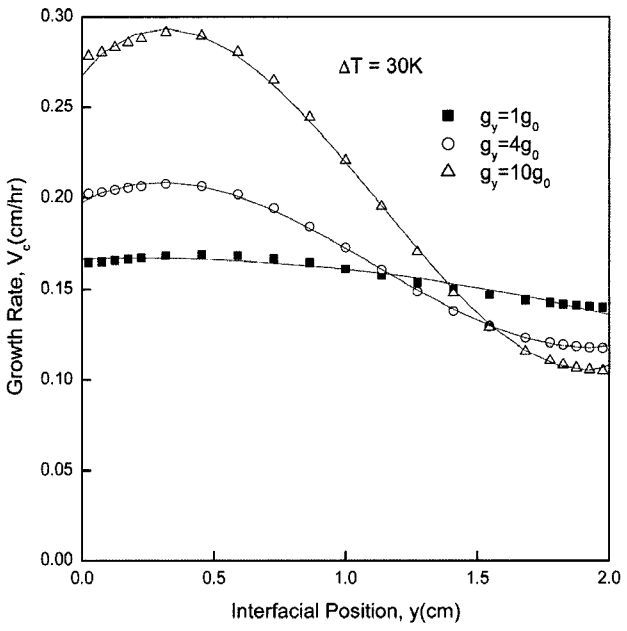

Fig. 5. Interfacial distributions of crystal growth rate of Hg_2Cl_2 for various gravity accelerations, at $\Delta T = 30$ K and $P_B = 20$ Torr. Based on Ar = 5.0, Pr = 0.81, Le = 0.34, $Gr_t = 8.4 \times 10^3$, $Gr_s = 9.7 \times 10^4$, Pe = 2.38, $C_v = 1.1$, $g_y = 1g_0$.

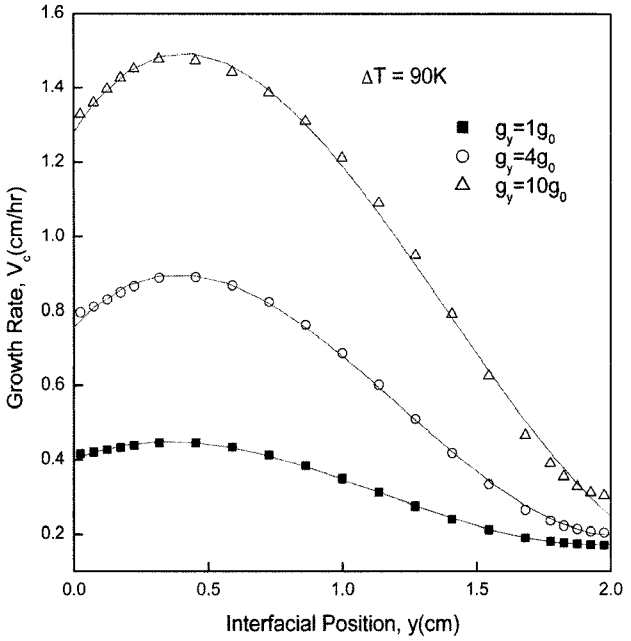

Fig. 6. Interfacial distributions of crystal growth rate of Hg_2Cl_2 for various gravity accelerations, at $\Delta T = 90$ K and $P_B = 20$ Torr. Based on Ar = 5.0, Pr = 0.78, Le = 0.5, $Gr_t = 5.6 \times 10^4$, $Gr_s = 4.0 \times 10^5$, Pe = 4.13, $C_v = 1.1$, $g_y = 1g_0$.

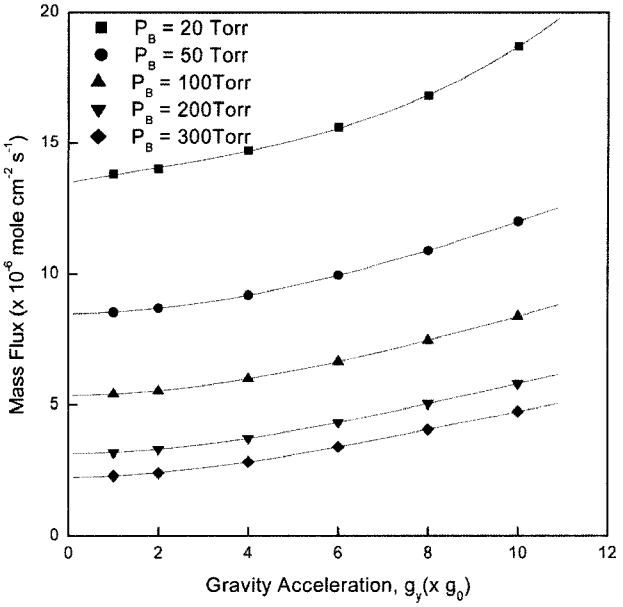

Fig. 7. Effects of partial pressure of component B, P_B (Torr) on the mass flux of Hg_2Cl_2 in terms of mole $cm^{-2}s^{-1}$ for various gravity accelerations of $1g_0 \le g_y \le 10g_0$ for the horizontal orientations and the temperature differences between the source and the crystal region of 320°C → 290°C, Ar = 5, L = 10 cm, with the linear temperature profiles at walls.

Fig. 4 shows the relationships between the growth rate and the gravity accelerations for three temperature differences between the source and the crystal regions, corresponding to Fig. 2. Fig. 4 is prepared from viewpoint of the crystal growth rate (cm/hr) to provide a good frame for Figs. 5 and 6, which show interfacial distributions of crystal growth rate of Hg_2Cl_2 for various gravity accelerations, at $\Delta T = 30$ K and 90 K, respectively. As shown in Fig. 5, the interfacial distributions for three gravity accelerations of $1g_0$, $4g_0$, and $10g_0$ are relatively flat after y = 1.3 cm. The maximum growth rates for three cases appear approximately in the neighborhood of y = 0.5, and the growth rates shows asymmetrical patterns, which indicate the occurrence of either one single or more than one convective cell. At y = 0.5, the maximum growth rate for $10g_0$ is nearly greater than for $1g_0$ by a factor of 2. Near at y = 2.0 the growth rates follow in the order of $10g_0 < 4g_0 < 1g_0$, which reflect intensive convective flow fields with increasing the gravity acceleration up to $10g_0$. As shown in Fig. 6, like the cases of $\Delta T = 30$ K the maximum growth rates for three gravity accelerations appear at in the neighborhood of y = 0.5, and the growth rates versus the interfacial positions show asymmetrical against at y = 1.0. The growth rates for three different gravities of 1, 4, $10g_0$ approach at the neighborhood of 0.3. Unlike the cases of $\Delta T = 30$ K, the near at y = 2.0 the growth rates for $\Delta T = 90$ K follow in the order of $1g_0 < 4g_0 < 10g_0$. In comparisons of Fig. 5 with Fig. 6, this discrepancy between $\Delta T = 30$ K and 90 K is likely to be due to the fact that near at y = 2.0 the patterns of growth rates for $\Delta T = 90$ K are more convection-dominated than for $\Delta T = 30$ K. As shown in Fig. 5, for $\Delta T = 30$ K and $10g_0$, the maximum growth rate is greater than the minimum growth rate by a factor of 2.7. On the other hand, as shown in Fig. 6, for $\Delta T = 90$ K and $10g_0$, the maximum growth rate is greater than the minimum growth rate by a factor of 4.9. Therefore, the deviation between the maximum and the minimum growth rate for $\Delta T = 90$ K and $10g_0$ is greater than for $\Delta T = 30$ K by a factor of 2, which indicate the mass transport is convection-dominated with increasing the temperature difference.

Fig. 7 shows effects of partial pressure of component B, P_B (Torr) on the mass flux of Hg_2Cl_2 in terms of mole $cm^{-2}s^{-1}$ for various gravity accelerations of $1g_0 \le g_y \le 10g_0$ for the horizontal orientations and the temperature differences between the source and the crystal region of 320°C → 290°C, Ar = 5, L = 10 cm, with the linear temperature profiles at walls. As shown in Fig. 7, the mass flux increases with increasing the gravity acceleration, for $1g_0 \le g_y \le 10g_0$, and decreases with increasing the partial pressure of component B, xenon (Xe), P_B. It is clear to see that as the P_B increases, the gap between the polynomial regression lines is decreased. Fig. 8 shows the $|U|_{max}$ as a function of gravity accelera-

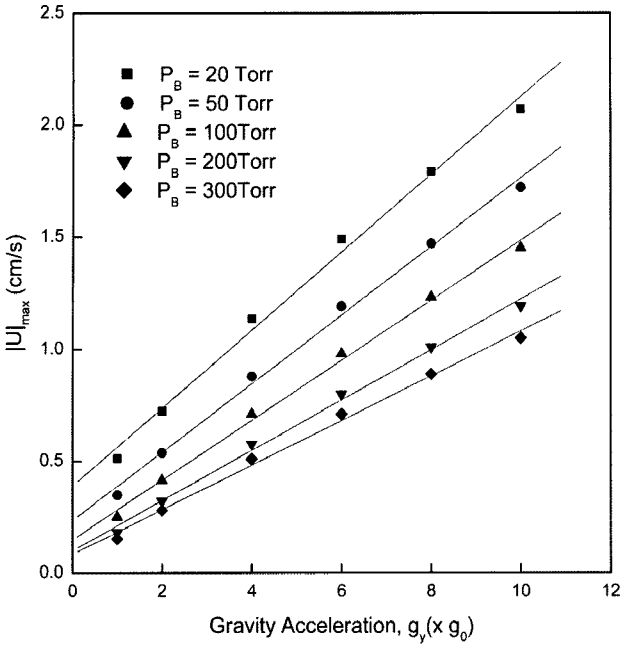

Fig. 8. The $|U|_{max}$ as a function of gravity accelerations for various partial pressures of P_B (Torr), 20 Torr $\leq P_B \leq$ 300 Torr, corresponding to Fig. 7.

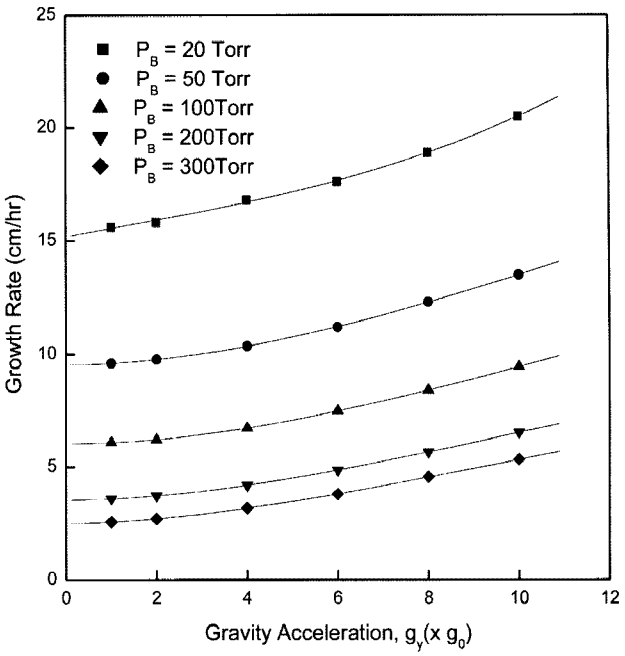

Fig. 9. The crystal growth rate of Hg_2Cl_2 as a function of gravity accelerations for various partial pressures of P_B (Torr), 20 Torr $\leq P_B \leq$ 300 Torr, corresponding to Fig. 7.

tions for various partial pressures of P_B (Torr), 20 Torr P_B 300 Torr, corresponding to Fig. 7. The $|U|_{max}$ is directly proportional to the gravity acceleration for 20 Torr P_B 300 Torr. As the partial pressure of P_B (Torr) decreases from 300 Torr to 20 Torr, the slope of the $|U|_{max}$ versus the gravity acceleration increases from 0.1 sec to 0.17 sec. For the gravity accelerations under consideration, the gap between the polynomial regression lines of the $|U|_{max}$ is the smallest at $g_y = 1g_0$. In other words, at $g_y = 10g_0$, as the P_B (Torr) is increased from 20 Torr to 300 Torr, i.e. by a factor of 15, the $|U|_{max}$ is decreased from 2.0 cm s^{-1} to 1.0 cm s^{-1} by a factor of 0.5. On the other hand, at $g_y = 1g_0$, as the P_B (Torr) is increased from 20 Torr to 300 Torr, i.e. by a factor of 15, the $|U|_{max}$ is decreased from 0.5 cm s^{-1} to 1.5 cm s^{-1} by a factor of 0.33. Therefore, as the gravity level is decreased from $1g_0$ to $10g_0$, the ratio of factors for $|U|_{max}$ is approximately 1.5, i.e. a factor of 0.5 to a factor of 0.33. Fig. 9 shows the crystal growth rate of Hg_2Cl_2 as a function of gravity accelerations for various partial pressures of P_B (Torr), 20 Torr $\leq P_B \leq$ 300 Torr, corresponding to Fig. 7. The growth rate increases the third order polynomially with the gravity level for 20 Torr $\leq P_B \leq$ 300 Torr. At $g_y = 10g_0$, as the P_B (Torr) is increased from 20 Torr to 300 Torr, i.e. by a factor of 15, the growth rate is decreased from 0.2 cm hr^{-1} to 0.05 cm hr^{-1} by a factor of 0.25. On the other hand, at $g_y = 1g_0$, as the P_B (Torr) is increased from 20 Torr to 300 Torr, i.e. by a factor of

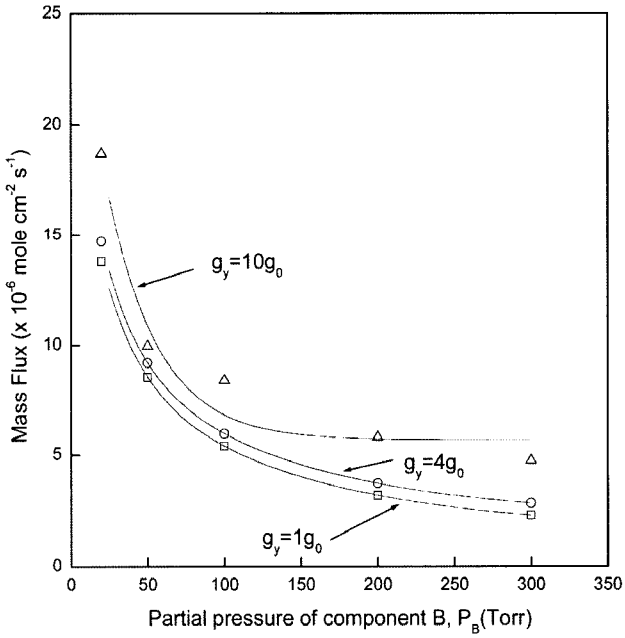

Fig. 10. The mass flux of Hg_2Cl_2 in terms of mole $cm^{-2}s^{-1}$ as a function of partial pressure of component B, P_B (Torr) for three gravity accelerations of $g_y = 1g_0$, $4g_0$ and $10g_0$, corresponding to Fig. 7.

15, the growth rate is decreased from 0.15 cm hr^{-1} to 2.5 cm hr^{-1} by a factor of 0.06. Therefore, as the gravity level is decreased from $1g_0$ to $10g_0$, the ratio of factors for the growth rate is approximately 4, i.e. a factor of 0.25 to a factor of 0.06. Fig. 10 shows the mass flux of Hg_2Cl_2 in terms of mole $cm^{-2}s^{-1}$ as a function of par-

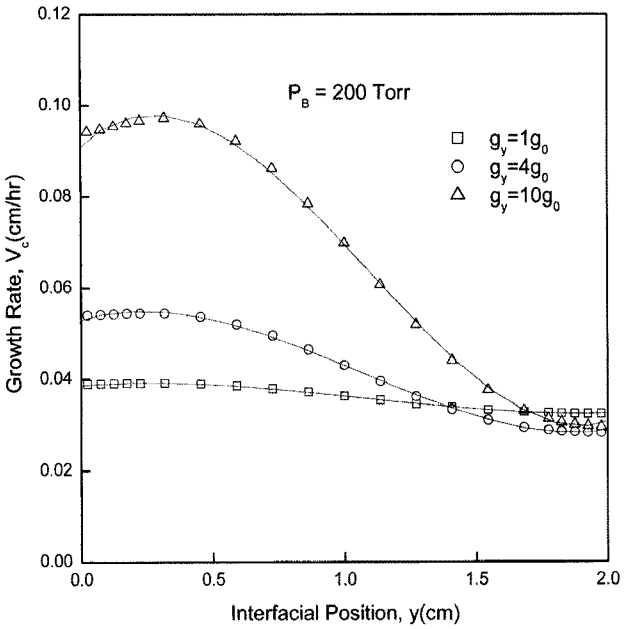

Fig. 11. Interfacial distributions of crystal growth rate of Hg_2Cl_2 for various gravity accelerations, at $\Delta T = 30$ K and $P_B = 200$ Torr. Based on Ar = 5.0, Pr = 0.74, Le = 0.59, $Gr_t = 1.4 \times 10^3$, $Gr_s = 1.1 \times 10^5$, Pe = 0.8, $C_v = 1.8$, $g_y = 1g_0$.

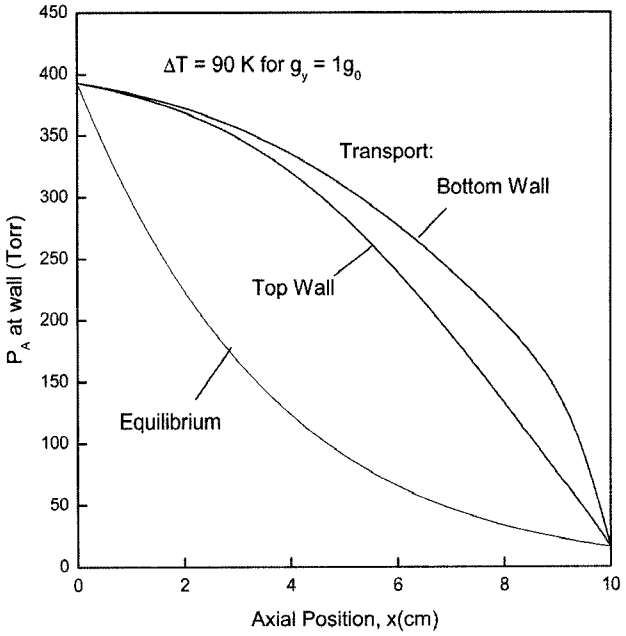

Fig. 12. Axial distribution of partial pressures of component A (Hg_2Cl_2) at the walls resulting from diffusive-convective transport at $g_y = 1g_0$, $\Delta T = 90$ K (350°C → 260°C) and equilibrium vapor pressure profile corresponding to the linear wall temperature distribution. Based on Ar = 5, $P_B = 20$ Torr, Ar = 5, L = 10 cm.

tial pressure of component B, P_B (Torr) for three gravity accelerations of $g_y = 1g_0$, $4g_0$, $10g_0$, corresponding to Fig. 7. The mass flux of Hg_2Cl_2 decreases exponentially with increasing the partial pressure of component B, P_B (Torr) from 20 Torr up to 300 Torr. Near at P_B = 20 Torr, the mass flux decreases sharply and, then since $P_B = 100$ Torr, decreases slowly until at $P_B = 300$ Torr. At $g_y = 10g_0$, the decrease in the mass flux appears relatively small for 100 Torr ≤ P_B ≤ 300 Torr. Figs. 5 and 12 show the interfacial distributions of crystal growth rate of Hg_2Cl_2 for various gravity accelerations, at $P_B = 20$ Torr and 200 Torr, respectively. For the case of $g_y = 1g_0$, $P_B = 20$ Torr and $\Delta T = 30$ K in Fig. 5, the corresponding parameters are as follows: Ar = 5.0, Pr = 0.81, Le = 0.34, $Gr_t = 8.4 \times 10^3$, $Gr_s = 9.7 \times 10^4$, Pe = 2.38, $C_v = 1.1$. As shown in Fig. 11, like the cases of $P_B = 20$ Torr, in Fig. 5, the maximum growth rates for three gravity accelerations appear at the neighborhood of y = 0.5, and the growth rates versus the interfacial positions show asymmetrical against at y = 1.0. The growth rates for three different gravities of 1, 4 and 10 g_0 approach at the neighborhood of 0.043. Unlike the cases of $P_B = 20$ Torr, the near at y = 2.0 the growth rates for $P_B = 200$ Torr follow in the order of $4g_0 < 10g_0 < 1g_0$. In comparisons of Fig. 5 with Fig. 11, this discrepancy between $P_B = 20$ Torr and 200 Torr is likely to be due to the fact that near at y = 2.0 the patterns of growth rates for P_B = 20 Torr are more convection-dominated than for P_B = 200 Torr. The maximum growth rate for $P_B = 20$ Torr and $10g_0$ in Fig. 5 is greater than the minimum growth rate by a factor of 2.7. On the other hand, the maximum growth rate for $P_B = 200$ Torr and $10g_0$ in Fig. 5 is greater than the minimum growth rate by a factor of 3.34. Therefore, the deviation between the maximum and the minimum growth rate for $P_B = 200$ Torr and $10g_0$ is greater than for $P_B = 20$ Torr by a factor of 1.23, which implies the mass transport is convection-dominated with increasing the partial pressure of component B, P_B.

Fig. 12 shows the axial distribution of partial pressures of component A(Hg_2Cl_2) at the walls resulting from diffusive-convective transport at $g_y = 1g_0$, $\Delta T = 90$ K (350°C → 260°C) and equilibrium vapor pressure profile corresponding to the linear wall temperature distribution. In Fig. 12, we compare the equilibrium profile with the $p_A(y)$s that arise at the bottom and the top walls due to diffusive-convective transport at $1g_0$. It should be noted that the higher concentration along the bottom wall, again reflecting the counter-clockwise sense of rotation of the thermal and/or solutal convection. The vapor of component A (Hg_2Cl_2) is in the supersaturated state throughout the ampoule in both cases, so it is easy to see why a linear temperature profile is rarely used in practice.

4. Conclusions

The roles of convection in crystal growth of Hg_2Cl_2-Xe can be enlarged in physical vapor transport systems for normal and high gravity environments. A gravitational acceleration level of more than $1g_0$ can be adequate to ensure diffusive-convection transport. The operating conditions under consideration in this study are Ar = 5, P_B = 20 Torr, Ar = 5, L = 10 cm, ΔT = 90 K and $g_y = 1g_0$, with the linear temperatures on the walls. The governing dimensionless parameters are as follows: Ar = 5.0, Pr = 0.78, Le = 0.5, $Gr_t = 5.6 \times 10^4$, $Gr_s = 4.0 \times 10^5$, Pe = 4.13, C_v = 1.1. For both ΔT = 60 K and 90 K, the mass flux increases by a factor of 3 with increasing the gravity acceleration from $1g_0$ up to $10g_0$. On the other hand, for ΔT = 30 K, the flux is increased by a factor of 1.36 for the range of $1g_0 \le g \le 10g_0$. Consequently, under the conditions of high gravity accelerations, the mass fluxes for both ΔT = 60 K and 90 K are approximately greater than the flux at ΔT = 30 K by a factor of 2. The maximum growth rates for for $1g_0$, $4g_0$ and $10g_0$ appear approximately in the neighborhood of y = 0.5, and the growth rates shows asymmetrical patterns, which indicate the occurrence of either one single or more than one convective cell. The maximum growth rate for $10g_0$ is nearly greater than that for $1g_0$ by a factor of 2.0 at P_B = 20 Torr. For three different gravity levels of $1g_0$, $4g_0$ and $10g_0$, the maximum growth rates are greater than the minimum rates by a factor of nearly 3.0 for P_B = 20 Torr. The mass flux increases with increasing the gravity acceleration, for $1g_0 \le g_y \le 10g_0$, and decreases with increasing the partial pressure of component B, xenon (Xe), PB. The $|U|_{max}$ is directly proportional to the gravity acceleration for 20 Torr $\le P_B \le$ 300 Torr. As the partial pressure of P_B (Torr) decreases from 300 Torr to 20 Torr, the slope of the $|U|_{max}$ versus the gravity acceleration increases from 0.1 sec to 0.17 sec. The mass flux of Hg_2Cl_2 is exponentially decayed with increasing the partial pressure of component B, P_B (Torr) from 20 Torr up to 300 Torr.

Acknowledgements

This paper has been supported by the 2009 Hannam University Research Fund (March 1, 2009 through February 28, 2010). One of the authors (Geug-Tae Kim) would like to thank the Hannam University for support of the current investigations through an one-year professor-yeonguneon program starting from September 1, 2008 at the Department of Materials Science & Engineering, University of Florida at Gainesville, Florida, USA.

References

[1] D.W. Greenwell, B.L. Markham and F. Rosenberger, "Numerical modeling of diffusive physical vapor transport in cylindrical ampoules", J. Crystal Growth 51 (1981) 413.

[2] B.L. Markham, D.W. Greenwell and F. Rosenberger, "Numerical modeling of diffusive-convective physical vapor transport in cylindrical vertical ampoules", J. Crystal Growth 51 (1981) 426.

[3] B.S. Jhaveri and F. Rosenberger, "Expansive convection in vapor transport across horizontal enclosures", J. Crystal Growth 57 (1982) 57.

[4] B.L. Markham and F. Rosenberger, "Diffusive-convective vapor transport across horizontal and inclined rectangular enclosures", J. Crystal Growth 67 (1984) 241.

[5] G.P. Extremet, P. Bontoux and B. Roux, "Effect of temperature gradient locally applied on a long horizontal cavity", Int'l. J. Heat and Fluid Flow 8 (1987) 26.

[6] A. Nadarajah, F. Rosenberger and J. Alexander, "Effects of buoyancy-driven flow and thermal boundary conditions on physical vapor transport", J. Crystal Growth 118 (1992) 49.

[7] H. Zhou, A. Zebib, S. Trivedi and W.M.B. Duval, "Physical vapor transport of zinc-telluride by dissociative sublimation", J. Crystal Growth 167 (1996) 534.

[8] F. Rosenberger, J. Ouazzani, I. Viohl and N. Buchan, "Physical vapor transport revised", J. Crystal Growth 171 (1997) 270.

[9] N. Ramachandran, C.H. Su and S.L. Lehoczky, "Modeling studies of PVT growth of ZnSe: current status and future course", J. Crystal Growth 208 (2000) 269.

[10] C. Mennetrier and W.M.B. Duval, "Thermal-solutal convection with conduction effects inside a rectangular enclosure", NASA Technical Memorandum 105371 (1991).

[11] C. Mennetrier, W.M.B. Duval and N.B. Singh, "Physical vapor transport of mercurous chloride under a nonlinear thermal profile", NASA Technical Memorandum 105920 (1992).

[12] Jing Lu, Zi-Bing Zhang and Qi-Sheng Chen, "Numerical simulation of the flow field and concentration distribution in the bulk growth of silicon carbide crystals", J. Crystal Growth 292 (2006) 519.

[13] H. Wiedemeier and W. Palosz, "Vapor transport and crystal growth of GeSe under normal and high acceleration", J. Crystal Growth 119 (1992) 79.

[14] Edward R. Letts, James S. Speck and Shuji Nakamura, "Effect of indium on the physical vapor transport growth of AlN", J. Crystal Growth 311 (2009) 1060.

[15] D. Zhuang, Z.G. Herro, R. Schlesser and Z. Sitar, "Seeded growth of AlN single crystals by physical vapor transport", J. Crystal Growth 287 (2006) 372.

[16] J.-S. Kim, Sudhir B. Trivedi, Jolanta Soos, Neelam Gupta and Witold Palosz, "Growth of Hg_2Cl_2 and

Hg_2Br_2 single crystals by physical vapor transport", J. Crystal Growth 310 (2008) 2457.

[17] N.B. Singh, W.M.B. Duval, A.S. W. Thomas, M.E. Glicksman, J.D. Adam, H. Zhang, J.C. Goldmbeck, C. Watson, R. Naumman, A.E. Nelson, C. Cacioppo, J. Griffin, M. Jugrav, T. Rolin, J. Seaquist and N. Daniel, "Microgravity experiment to understand the effect of convection on PVT crystal growth", Adv. Space Res. 32 (2003) 211.

[18] C.-H. Su, S. Feth and S.L. Lehoczky, "*In situ* partial pressure measurements and visual observation during crystal growth of ZnSe by seeded physical vapor transport", J. Crystal Growth 209 (2000) 687.

[19] C.-H. Su, M.A. George, W. Palosz, S. Feth and S.L. Lehoczky, "Contactless growth of ZnSe single crystals by physical vapor transport", J. Crystal Growth 213 (2000) 267.

[20] W. Palosz, "Physical vapor transport of lead telluride", J. Crystal Growth 216 (2000) 273.

[21] W.M.B. Duval, "Convection in the physical vapor transport process--I: Thermal convection", J. Chem. Vapor Deposition 2 (1994a) 188.

[22] W.M.B. Duval, "Convection in the physical vapor transport process--II: Thermosolutal convection", J. Chem. Vapor Deposition 2 (1994b) 282.

[23] W.M.B. Duval, "Transition to chaos in the physical vapor transport process--I: fluid mechanics problem phenomena in microgravity", Fluids Eng. Div. ASME 175 (1993) 51.

[24] W.M.B. Duval, N.E. Glicksman and B. Singh, "Physical vapor transport of mercurous chloride crystals; design of a microgravity experiment", J. Crystal Growth 174 (1997) 120.

[25] P.A. Tebbe, S.K. Loyalka and W.M.B. Duval, "Finite element modeling of asymmetric and transient flow flieds during physical vapor transport", Finite Elements in Analysis and Design 40 (2004) 1499.

[26] G.T. Kim, W.M.B. Duval, N.B. Singh and M.E. Glicksman, "Thermal convective effects on physcial vapor transport growth of mercurous chloride crystals (Hg_2C1_2) for axisymmetric 2-D cylindrical enclosure", Modelling. Simul. Mater. Sci. Eng. 3 (1995) 331.

[27] G.T. Kim, W.M.B. Duval and M.E. Glicksman "Thermal convection in physical vapour transport of mercurous chloride (Hg_2Cl_2) for rectangular enclosures", Modelling. Simul. Mater. Sci. Eng. 5 (1997) 289.

[28] G.T. Kim, W.M.B. Duval and M.E. Glicksman "Effects of asymmetric temperature profiles on thermal convection during physical vapor transport of Hg_2Cl_2", Chem. Eng. Comm. 162 (1997) 45.

[29] J.-G. Choi, K.-H. Lee, M.-H. Kwon and G.-T. Kim, "Effect of accelerational perturbations on physical vapor transport crystal growth under microgravity environments", J. Korean Crystal Growth and Crystal Technology 16 (2006) 203.

[30] G.-T. Kim and K.-H. Lee, "Parametric studies on convection during the physical vapor transport of mercurous chloride (Hg_2Cl_2)", J. Korean Crystal Growth and Crystal Technology 14 (2004) 281.

[31] G.T. Kim, "Convective-diffusive transport in mercurous chloride (Hg_2Cl_2) crystal growth", J. Ceramic Processing Research 6 (2005) 110.

[32] J.-G. Choi, K.-H. Lee and G.-T. Kim, "effects of inert gas (Ne) on thermal convection of mercurous chloride system of Hg_2Cl_2 and Ne during physical vapor transport", J. Korean Crystal Growth and Crystal Technology 18 (2008) 225.

[33] J.-G. Choi, K.-H. Lee and G.-T. Kim, "Generic studies on thermo-solutal convection of mercurous chloride system of Hg_2Cl_2 and Ne during physical vapor transport", J. Korean Crystal Growth and Crystal Technology 1 (2009) 39.

[34] N.B. Singh, R. Mazelsky and M.E. Glicksman, "Evaluation of transport conditions during PVT: mercurous chloride system", PhysicoChemical Hydrodynamics 11 (1989) 41.

[35] N.B. Singh, M. Gottlieb, G.B. Brandt, A.M. Stewart, R. Mazelsky and M.E. Glicksman, "Growth and characterization of mercurous halide crystals:mercurous bromide system", J. Crystal Growth 137 (1994) 155.

[36] N.B. Singh, R.H. Hopkins, R. Mazelsky and J.J. Conroy, "Purification and growth of mercurous chloride single crystals", J. Crystal Growth 75 (1970) 173.

[37] S.J. Yosim and S.W. Mayer, "The mercury-mercuric chloride system", J. Phys. Chem. 60 (1960) 909.

[38] F. Rosenberger and G. Müller, "Interfacial transport in crystal growth, a parameter comparison of convective effects", J. Crystal Growth 65 (1983) 91.

[39] S.V. Patankar, "Numerical heat transfer and fluid flow" (Hemisphere Publishing Corp., Washington D.C., 1980).